Supporting Information for

Programmable cyclic flow bioprocess enables in-situ anammox bacteria enrichment and advanced nitrogen removal from low C/N wastewater

Jiapeng Li 1,2, Xiaotian Zuo 1,2, Hanbin Wang 3, Huo Huang 4, Fangang Meng (✉)1,2

1 School of Environmental Science and Engineering, Sun Yat-sen University, Guangzhou 510275, China

2 Guangdong Provincial Key Laboratory of Environmental Pollution Control and Remediation Technology (Sun Yat-sen University), Guangzhou 510275, China

3 National Engineering Laboratory for Advanced Municipal Wastewater Treatment and Reuse Technology, Engineering Research Center of Beijing, Beijing University of Technology, Beijing 100124, China

4 School of Environmental and Chemical Engineering, Foshan University, Foshan 528000, China

Number of pages: 23

Number of methods: 4

Number of tables: 5

Number of Figures: 19

Supplementary Methods

Method S1 16S rRNA gene amplicon sequencing

✉ Corresponding author
E-mail: mengfg@mail.sysu.edu.cn

Method S2 Co-occurrence network construction

Method S3 Community assembly process analysis

Method S4 Metagenomic analysis

Method S5 Supplementary chemical analyses

Supplementary Tables

Table S1 The synthetic solutions used in the bath tests.

Table S2 Mass balance calculations for carbon, nitrogen and phosphorus based on the long-term monitoring in the reactor.

Table S3 Experiment conditions for functional bacterial activity batch tests.

Table S4 Microbial diversity index in flocs and biofilms at different period.

Table S5 Topological properties of the empirical and associated random pMENs of suspended sludge and biofilms communities. The small-world coefficient σ = (CC/CCr)/(HD/HDr), and subscript r indicates the characteristics of the random network.

Supplementary Figures

Fig. S1 Effluent TIN concentrations under different cycle durations.

Fig. S2 The nitrogen, phosphorus and COD profiles in the anoxic and oxic tanks of the novel continuous A/O process over a typical cycle in Phase I and Phase II.

Fig. S3 Reactor performance during the operation of 280 days. (a) The influent, effluent, and removal efficiency of COD; (b) The influent and effluent PO_4^{3-}-P; (c) The operating temperatures.

Fig. S4 The sludge concentrations of suspended sludge and carrier biofilms

Fig. S5 Specific variations of nitrogen and COD in batch tests. (a) The anammox batch tests of anoxic biofilms in Phase I; (b) The PDA batch tests of hybrid system from anoxic zone in Phase I; (c) The endogenous denitrification batch tests of suspended sludge in Phase II; (d) The SND batch tests of carrier biofilms from oxic zone in Phase II; (e) The SND batch tests of hybrid system from oxic zone in Phase II; (f) The anammox batch tests of anoxic biofilms in Phase III. (Note: Hybrid systems comprised both carrier biofilms and suspended sludge. Samples used for batch tests were collected on day 105 for Phase I, day 220 for Phase II, and day 250 for Phase III.)

Fig. S6 Microscopic visualization of suspended sludge and carrier biofilms based on the fluorescence images of live (green) and dead (red) cells.

Fig. S7 Mass balance calculations for nitrogen in Phase III and Phase IV of the novel modified continuous A/O process. r: nitrifying liquid reflux ratio [%]; R: sludge return ratio [%]; q: wasted sludge ratio [%]; Q: average influent flowrate [L/d]; N_{exp}: TIN in the wasted sludge; N_{eff}: TIN in the effluent; N_{PDA}: nitrogen loss by PDA; N_{SND}: nitrogen loss by SND; N_{CND}: nitrogen loss by CND in anoxic tank; $N_{settler}$: nitrogen in settler.

Fig. S8 Evolution of intracellular carbon sources. (a) The conversion of endogenous carbon sources (PHA, PHB, PHV) from anoxic tank to oxic tank; (b) Variations in the amount of PHA in phase I and phase II.
Fig. S9 Variation in the nitrification activity in the reactor. (a) Nitrification activity of aerobic carrier biofilms; (b) Nitrification activity of suspended sludge; (c) Nitrification activity of the hybrid system. (Note: the hybrid system contained aerobic carrier biofilms and suspended sludge.)
Fig. S10 Denitrification batch tests of the carrier biofilms (a) and the hybrid system (b) from anoxic tank. (Note: the hybrid system contained anoxic carrier biofilms and suspended sludge.)
Fig. S11 Results of the principal coordinates analysis (PCoA) at the ASV level.
Fig. S12 Microbial community structure at the phylum level from suspended sludge (a), carrier biofilms from anoxic tank (b) and oxic tank (c).
Fig. S13 Profile of the nitrogen-cycle genes in *Haliangiaceae* genome.
Fig. S14 The key genes involved in denitrification and nitrification processes in suspended sludge and aerobic biofilms. (a) Variations in the relative abundance of functional genes. (b) Variations in the relative abundance of *nar* and *nap* genes in suspended sludge and aerobic biofilms. (c) Variations in the relative abundance of *nir* genes in suspended sludge and aerobic biofilms.
Fig. S15 Long-term dynamics of anammox activity in anoxic biofilms.
Fig. S16 Bacterial co-occurrence networks constructed from ASV-level Spearman correlations. Networks were generated based on pairwise Spearman correlation coefficients ($|r| > 0.7$, $P < 0.01$) among ASVs. Node size reflects the degree of connectivity (i.e., the number of significant associations). The top panels depict microbial interaction networks from suspended sludge in Phase I (a) and Phase II (b), while the bottom panels illustrate those from anoxic (c) and oxic (d) biofilms.
Fig. S17 Z−P plot of ASVs in microbiomes based on their topological roles. (a) Z−P plot of ASVs in suspended sludge from phase I. (b) Z−P plot of ASVs in suspended sludge from phase II. (c) Z−P plot of ASVs in anaerobic carrier biofilms. (d) Z−P plot of ASVs in aerobic carrier biofilms. The topological feature of each node was determined based on the scatter patterns of Zi and Pi.
Fig. S18 SND batch tests conducted at a dissolved oxygen concentration of 1.4-1.5 mg O_2/L. (a) SND activity of hybrid system from oxic tank in Phase I; (b) SND activity of hybrid system from oxic tank in Phase II. (Note: Hybrid systems comprised both carrier biofilms and suspended sludge. Samples used for batch tests were collected on day 105 for Phase I and on day 220 for Phase II.)
Fig. S19 Microbial co-occurrence networks of specie *Ca. Brocadia sapporoensis* based on pairwise Spearman's correlations among ASVs. With only significant associations ($P < 0.01$ and correlation coefficient >|0.7|) included. Nodes size is scaled according to the number of connections (degree).

Nomenclature

Anammox	*anaerobic ammonium oxidation*
AOB	*ammonia oxidizing bacteria*
NOB	*nitrite oxidizing bacteria*
COD	*chemical oxygen demand*
PDA	*partial denitrification and anammox*
C_{inf}	*COD in the influent*

C_{eff}	*the fraction of influent COD remaining in the effluent*
C_{exp}	*the fraction of influent COD associated with wasted sludge*
$C_{removal}$	*the COD removal efficiency of the system*
C_{AN}	*the fraction of COD removed in the anoxic tank*
C_{O}	*the fraction of COD removed in the oxic tank*
$C_{settler}$	*the fraction of COD removed in the settler*
C_{SDN-O}	*the fraction of COD used for SND in the oxic tank*
MLSS	*mixed liquor suspended solid*
MLVSS	*mixed liquor volatile suspended solid*
N_{inf}	*TIN in the influent*
N_{eff}	*the fraction of influent TIN remaining in the effluent*
N_{exp}	*the fraction of influent TIN associated with wasted sludge*
$N_{removal}$	*the TIN removal efficiency of the system*
N_{An}	*the fraction of TIN removed in the anoxic tank*
N_{SND}	*the fraction of TIN removed by SND in the anoxic tank*
N_{PDA}	*the fraction of TIN removed by PDA in the anoxic tank*
$N_{settler}$	*the fraction of TIN removed in the settler*
P_{inf}	*PO_4^{3-}-P in the influent*
P_{eff}	*the fraction of influent PO_4^{3-}-P remaining in the effluent*
P_{exp}	*the fraction of influent PO_4^{3-}-P associated with wasted sludge*
$P_{removal}$	*the PO_4^{3-}-P removal efficiency of the system*
P_{AN}	*the fraction of PO_4^{3-}-P removed in the anoxic tank*
P_{O}	*the fraction of PO_4^{3-}-P removed in the oxic tank*
$P_{settler}$	*the fraction of PO_4^{3-}-P removed in the settler*
Q	*average influent flowrate [L/d]*
q	*wasted sludge ratio [%]*
r	*nitrifying liquid reflux ratio [%]*
R	*Sludge return ratio [%]*
$S_{COD-AN-eff}$	*COD in the anoxic tank [mg/L]*
$S_{COD-O-eff}$	*COD in the oxic tank [mg/L]*
$S_{COD-eff}$	*COD in the effluent [mg/L]*
$S_{COD-inf}$	*COD in the influent [mg/L]*
SND	*simultaneous nitrification-denitrification*
$S_{TIN-An-eff}$	*TIN in the effluent of anoxic tank [mg/L]*
$S_{TIN-O-eff}$	*TIN in the effluent of oxic tank [mg/L]*
$S_{TIN-eff}$	*TIN in the effluent [mg/L]*
$S_{TIN-inf}$	*TIN in the influent [mg/L]*
$S_{P-An-eff}$	*PO_4^{3-}-P in the effluent of anoxic tank [mg/L]*
S_{P-eff}	*PO_4^{3-}-P in the effluent [mg/L]*

$S_{P\text{-}inf}$	*PO_4^{3-}-P in the influent [mg/L]*
$S_{P\text{-}O\text{-}eff}$	*PO_4^{3-}-P in the effluent of oxic tank [mg/L]*
$S_{NH4\text{-}inf}$	*NH_4^+-N in the influent [mg/L]*
$S_{NH4\text{-}eff}$	*NH_4^+-N in the effluent [mg/L]*
$S_{NH4\text{-}O\text{-}eff}$	*NH_4^+-N in the effluent of oxic tank [mg/L]*
$S_{NH4\text{-}An\text{-}eff}$	*NH_4^+-N in the effluent of anoxic tank [mg/L]*
TIN	*total inorganic nitrogen*
WWTP	*wastewater treatment plant*

Method S1 16S rRNA gene amplicon sequencing

The DNA was extracted using the Fast DNA SPIN extraction kits (MP Biomedicals, Santa Ana, CA, USA) according to the manufacturer's protocols. The V3-V4 hypervariable regions of the bacteria 16S rRNA gene were amplified using the primers 338F (5'-ACTCCTACGGGAGGCAGCA-3') and 806R (5'-GGACTACHVGGGTWTCTAAT-3'). Purified amplicons were pooled in equimolar ratios and paired-end sequenced (2 × 250) on the Illumina NovaSeq platform with the NovaSeq 6000 SP Reagent Kit at Shanghai Personal Biotechnology Co., Ltd. (Shanghai, China). The sequences were rarefied to the lowest sequencing depth of 33109 sequences per sample. Raw sequences were processed within the QIIME2 pipeline using the DADA2 method to generate amplicon sequence variants (ASVs). The taxonomic annotation was conducted using feature classifier plugin with the SILVA SSU database (version 138). The raw reads were deposited into the NCBI Sequence Read Archive database under accession number PRJNA1302167.

Method S2 Co-occurrence network construction

For network analysis, a co-occurrence network was constructed based on Spearman's rank correlation between ASVs with sequences. The phylogenetic molecular ecological networks (pMENs) of sludge samples were constructed to characterize bacterial interactions using the random matrix theory (RMT)−based approach. pMEN construction and visualization were performed using the MEN analysis pipeline (http://ieg2.ou.edu/MENA) and Gephi 0.10.1 (WebAtlas, Paris, France), respectively.

Method S3 Community assembly process analysis

To evaluate the regulation of community assembly by an ecology-based control strategy, a neutral community model (NCM) was used to quantitatively predict the assembly patterns of sludge communities. The NCM was performed on the Tutools platform (https://www.cloudtutu.com). In this model, N_m and R^2 values represent the metacommunity size times immigration and the overall goodness-of-fit of the NCM, respectively. The community assembly processes were quantitatively estimated based on β-nearest taxon index (*β*NTI) and Bray-Curtis based Raup-Crick (R_{Cbray}). If |βNTI|≥2, pairwise comparisons were considered statistically significant and estimated as the influence of selection. Then, comparisons with nonsignificant βNTI values (|βNTI| < 2) were further estimated by RC_{bray}. The influence of ecological drift was estimated by $|RC_{bray}| \leq 0.95$. In addition, $RC_{bray} > +0.95$ and $RC_{bray} < -0.95$ represented dispersal limitation and homogenizing dispersal, respectively

Method S4 Metagenomic analysis

Metagenomic sequencing was conducted on the Illumina NovaSeq 6000 platform (Illumina Inc, US) with PE150 strategy at Personal Biotechnology Co., Ltd. (Shanghai, China). Of note, the sludge samples for metagenomic sequencing were collected on Days 1, 17 and 86. Trimmomatic (v0.39) was used to remove sequencing adapters, low-quality reads, and host contamination from raw sequences for obtaining clean reads (Bolger et al., 2014). Afterwards, these clean reads were *de novo* assembled to construct the metagenome for each biomass sample by MEGAHIT and only the assembled contigs with a minimum length of 1000 bp were further analyzed. Open reading frames (ORFs) were predicted using Prodigal (v2.6.3) in metagenome mode (Hyatt et al., 2010). Abundance of the contigs were calculated based on Transcripts Per Kilobase Million (TPM) values. Nitrogen cycling genes were annotated using NCycDB (Tu et al., 2019). The raw metagenomic data were deposited into the NCBI Sequence Read Archive database under accession number PRJNA1302710 and PRJNA1459653.

Genome binning process was conducted using three independent methods (including MetaBAT2 (Kang et al., 2019), MaxBin2 (Wu et al., 2016) and CONCOCT (Alneberg et al., 2014))

with the minimum contig length of 1000. After refined through the MetaWRAP pipeline, non-redundant MAGs were generated using dRep (Olm et al., 2017) with options of dereplicate_wf -sa 0.95 -comp 70 -con 10. The taxonomic information of non-redundant MAGs was obtained using the GTDB-Tk toolkit (Chaumeil et al., 2020) based on Genome Taxonomy DataBase (GTDB) (Parks et al., 2022) (release 83). Open Reading Frames (ORFs) were predicted for the contigs involved in each MAG using Prodigal (Hyatt et al., 2010). Nitrogen cycling genes were annotated using NCycDB (Tu et al., 2019).

Method S5 Supplementary chemical analyses

Glycogen (Gly) and poly-hydroxyalkanoates (PHA), including poly-β-hydroxybutyrate (PHB) and poly-β-hydroxyvalerate (PHV), were detected by gas chromatography (7890 A, Agilent, USA) from samples with freeze-dried preparation (Meng et al., 2020). The LIVE/DEAD BacLight bacterial viability kit containing SYTO 9 and propidium iodide was used to stain live and dead cells in the suspended sludge and biofilms (Yuan et al., 2022). The stained biofilm samples were observed by fluorescence microscopy using a model MF31microscope (Guangzhou Micro-shot Technology Co., Ltd.).

Table S1 The synthetic solutions used in the bath tests and influent.

Solutions	Concentration	Unit
Mineral element		
$KHCO_3/NaHCO_3$	500	mg/L
KH_2PO_4	27.2	mg/L
$MgSO_4 \cdot 7H_2O$	300	mg/L
$CaC1_2 \cdot 2H_2O$	180	mg/L
Trace element 1		
EDTA	5	g
$FeSO_4$	5	g
Trace element 2		
EDTA	15	g
$ZnSO_4 \cdot 7H_2O$	0.43	g
$CoC1_2 \cdot 6H_2O$	0.24	g
$MnC1_2 \cdot 4H_2O$	0.99	g
$CuSO_4 \cdot 5H_2O$	0.25	g
$NaMoO_4 \cdot 2H_2O$	0.22	g
$NiC1_2 \cdot 6H_2O$	0.19	g
$NaSeO_4 \cdot 10H_2O$	0.21	g
H_3BO_4	0.014	g

Table S2 Mass balance calculations for carbon, nitrogen and phosphorus based on the long-term monitoring in the reactor.

Mass	Parameters	Calculations	Phase I (%)	Phase II (%)	Phase III (%)	Phase IV (%)
Phosphorus	P_{inf}	$S_{P\text{-}inf}\times Q/S_{P\text{-}inf}\times Q$	100%	100%	100%	100%
	P_{eff}	$[(1-q)\times Q\times S_{P\text{-}eff}]/S_{P\text{-}inf}\times Q$	53.9±3.2	80.5±0.3	86.8±2.9	78.4±3.0
	P_{exp}	$q\times S_{P\text{-}eff}\times Q/S_{P\text{-}inf}\times Q$	0.9±0.1	1.4±0.0	1.5±0.0	1.3±0.1
	$P_{removal}$	$(S_{P\text{-}inf}-S_{P\text{-}eff})\times Q/S_{P\text{-}inf}\times Q$	45.2±3.3	18.1±0.4	11.7±2.9	20.3±3.0
	P_{AN}	$[(1+r+R)\times Q\times[(S_{P\text{-}inf}+RS_{P\text{-}eff}+rS_{P\text{-}O\text{-}eff})/(1+r+R)-S_{P\text{-}An\text{-}eff}]]/(S_{P\text{-}inf}-S_{P\text{-}eff})\times Q$	-46.2±3.6	-39.3±2.4	-244.9±118.3	-77.3±12.6
	P_{O}	$(1+r+R)\times Q\times(S_{P\text{-}An\text{-}eff}-S_{P\text{-}O\text{-}eff})/(S_{P\text{-}inf}-S_{P\text{-}eff})\times Q$	117.5±28.9	159.5±0.7	420.1±119.7	191.8±25.8
	$P_{settler}$	$[(1+R)\times Q\times(S_{P\text{-}O\text{-}eff}-S_{P\text{-}eff})]/(S_{P\text{-}inf}-S_{P\text{-}eff})\times Q$	28.7±25.3	-20.2±3.2	-75.2±1.4	-14.5±13.2
Nitrogen	N_{inf}	$S_{TIN\text{-}inf}\times Q/S_{TIN\text{-}inf}\times Q$	100%	100%	100%	100%
	N_{eff}	$(1-q)\times Q\times S_{TIN\text{-}eff}/S_{TIN\text{-}inf}\times Q$	5.4±0.9	15.7±0.4	21.6±0.0	17.1±0.0
	N_{exp}	$q\times S_{TIN\text{-}eff}\times Q/S_{TIN\text{-}inf}\times Q$	0.1±0.0	0.3±0.0	0.4±0.0	0.3±0.0
	$N_{removal}$	$(S_{TIN\text{-}inf}-S_{TIN\text{-}eff})\times Q/S_{TIN\text{-}inf}\times Q$	94.5±0.9	84.0±0.4	78.0±0.0	82.6±0.0
	N_{AN}	$[(1+r+R)\times Q\times[(S_{TIN\text{-}inf}+RS_{TIN\text{-}eff}+rS_{TIN\text{-}O\text{-}eff})/(1+r+R)-S_{TIN\text{-}An\text{-}eff}]]/(S_{TIN\text{-}inf}-S_{TIN\text{-}eff})\times Q$	24.1±3.1	68.9±9.0	71.8±0.8	72.3±1.4
	N_{SND}	$[(1+r+R)\times Q\times(S_{TIN\text{-}An\text{-}eff}-S_{TIN\text{-}O\text{-}eff})]/(S_{TIN\text{-}inf}-S_{TIN\text{-}eff})\times Q$	71.1±1.6	31.0±10.6	27.7±0.2	28.4±1.6
	$N_{settler}$	$[(1+R)\times Q\times(S_{TIN\text{-}O\text{-}eff}-S_{TIN\text{-}eff})]/(S_{TIN\text{-}inf}-S_{TIN\text{-}eff})\times Q$	4.8±4.7	0.1±1.6	0.5±1.0	-0.7±0.1
COD	C_{inf}	$S_{COD\text{-}inf}\times Q/S_{COD\text{-}inf}\times Q$	100%	100%	100%	100%
	C_{eff}	$(1-q)\times S_{COD\text{-}eff}\times Q/S_{COD\text{-}inf}\times Q$	5.7±1.0	12.0±2.2	14.5±0.3	15.5±0.0
	C_{exp}	$q\times S_{COD\text{-}eff}\times Q/S_{COD\text{-}inf}\times Q$	0.1±0.0	0.2±0.0	0.2±0.0	0.3±0.0
	$C_{removal}$	$(S_{COD\text{-}inf}-S_{COD\text{-}eff})\times Q/S_{COD\text{-}inf}\times Q$	94.2±1.0	87.8±2.2	85.3±0.3	84.2±0.0
	C_{AN}	$[(1+r+R)\times Q\times[(S_{COD\text{-}inf}+RS_{COD\text{-}eff}+rS_{COD\text{-}O\text{-}eff})/(1+r+R)-S_{COD\text{-}An\text{-}eff}]]/(S_{COD\text{-}inf}-S_{COD\text{-}eff})\times Q$	65.7±4.0	70.2±2.7	65.8±2.2	68.3±5.1
	C_{O}	$[(1+r+R)\times Q\times(S_{COD\text{-}An\text{-}eff}-S_{COD\text{-}O\text{-}eff})]/(S_{COD\text{-}inf}-S_{COD\text{-}eff})\times Q$	31.9±4.2	26.2±2.9	32.0±0.5	30.3±6.1
	$C_{settler}$	$[(1+R)\times Q\times(S_{COD\text{-}O\text{-}eff}-S_{COD\text{-}eff})]/(S_{COD\text{-}inf}-S_{COD\text{-}eff})\times Q$	2.4±0.2	3.6±0.2	2.2±2.6	1.4±1.0

C_{SND-O}	$2.86^a \times [(1+r+R) \times Q \times (S_{TIN-An-eff} - S_{TIN-O-eff})] / (S_{COD-inf} - S_{COD-eff}) \times Q$	36.7±1.1	27.1±9.2	21.7±0.3	24.5±1.4
N_{PDA}	$[2.06 \times (1+r+R) \times Q \times [(S_{NH4-inf} + RS_{NH4-eff} + rS_{NH4-O-eff}) / (1+r+R) - S_{NH4-An-eff}]] / (S_{TIN-inf} - S_{TIN-eff}) \times Q$	9.3±0.3	39.4±9.3	25.9±1.0	30.7±0.6
N_{CND}	$N_{AN} - N_{PDA}$	14.8±2.9	29.5±18.3	45.9±0.2	41.6±2.0

Influent samples were filtered for the determination of COD.

a. 2.86: *per gram N_2 generation consumes 2.86gCOD during the denitrification (NO_3^--N to N_2).*

In the batch tests, the percentage of anammox and denitrification contribution on nitrogen removal could be calculated in Eq. (S1) and Eq. (S2):

$$Anammox\ contribution\ (\%) = (\triangle NH_4^+\text{-}N) \times (1 + 1.32 - 0.26) \times 100\% / (\triangle TIN) \quad \text{(S1)}$$

$$Denitrification\ contribution\ (\%) = 100\% - Anammox\ contribution \quad \text{(S2)}$$

where, $\triangle NH_4^+\text{-}N_{inf}$ and $\triangle TIN$ represents the decreased amount of NH_4^+-N and TIN during the batch tests, respectively.

The percentage of SND contribution on nitrogen removal could be calculated in Eq. (S3).

$$SND\ contribution\ (\%) = (\triangle TIN) \times 100\% / (\triangle NH_4^+\text{-}N) \quad \text{(S3)}$$

Table S3 Experiment conditions for functional bacterial activity batch tests.

Bacteria	Initial pH	DO (mg O_2/L)	Initial ammonium (mg N/L)	Initial nitrite (mg N/L)
AOB	7.5-7.7	2.0-3.0	20	0
NOB	7.5-7.7	2.0-3.0	0	20
Anammox bacteria	7.5-7.7	0.01-0.03	20	20

Table S4 Microbial diversity index in flocs and biofilms at different period.

Sample	ace	chao	coverage	shannon	simpson
Floc-25	595.05	594.83	0.99992	4.80512	0.96984
Floc-125	605.89	605.31	0.99994	5.05591	0.98260
Floc-177	637.76	637.31	0.99988	5.17725	0.97621
Floc-240	635.48	635.33	0.99995	4.93695	0.97092
Floc-273	655.88	655.56	0.99987	4.84448	0.96696
Anoxic biofilm-100	563.74	563.40	0.99994	4.69218	0.97486
Anoxic biofilm-153	509.17	509.00	0.99998	4.55135	0.97001
Anoxic biofilm-200	536.43	536.05	0.99996	4.87754	0.98031
Anoxic biofilm-240	537.03	536.83	0.99993	4.73805	0.97599
Aerobic biofilm-50	634.18	632.54	0.99988	5.01896	0.97946
Aerobic biofilm-100	591.89	591.00	0.99978	4.71670	0.96731
Aerobic biofilm-177	589.35	588.33	0.99992	4.83600	0.97391
Aerobic biofilm-240	604.31	602.55	0.99983	4.99342	0.98031

Table S5 Topological properties of the empirical and associated random pMENs of suspended sludge and biofilms communities. The small-world coefficient σ = (CC/CCr)/(HD/HDr), and subscript r indicates the characteristics of the random network.

Samples	Empirical networks											Random networks		
	Network size (n)	Positive Links	Negative Links	Similarity threshold (St)	R^2 of power law	Average degree (avgK)	Harmonic geodesic distance (HD)	Average path distance (GD)	Average clustering coefficient (avgCC)	Transitivity (Trans)	Modularity	Average σ	Average clustering coefficient (avgCC±SD)	Harmonic geodesic distance (HD±SD)	Modularity (M±SD)
Suspended sludge in phase I	307	679	473	0.960	0.866	7.505	4.220	6.032	0.378	0.348	0.638	3.387	0.073 +/- 0.007	2.760 +/- 0.020	0.307 +/- 0.004
Suspended sludge in phase II	490	1566	675	0.960	0.802	9.147	4.426	5.833	0.329	0.353	0.562	2.466	0.084 +/- 0.006	2.787 +/- 0.013	0.263 +/- 0.004
Carrier biofilms from anoxic tank	379	740	449	0.960	0.879	6.274	4.895	7.094	0.235	0.333	0.668	2.787	0.052 +/- 0.006	3.019 +/- 0.022	0.352 +/- 0.004
Carrier biofilms from oxic tank	398	1074	462	0.960	0.825	7.719	4.330	5.680	0.297	0.229	0.688	3.252	0.060 +/- 0.006	2.845 +/- 0.014	0.306 +/- 0.004

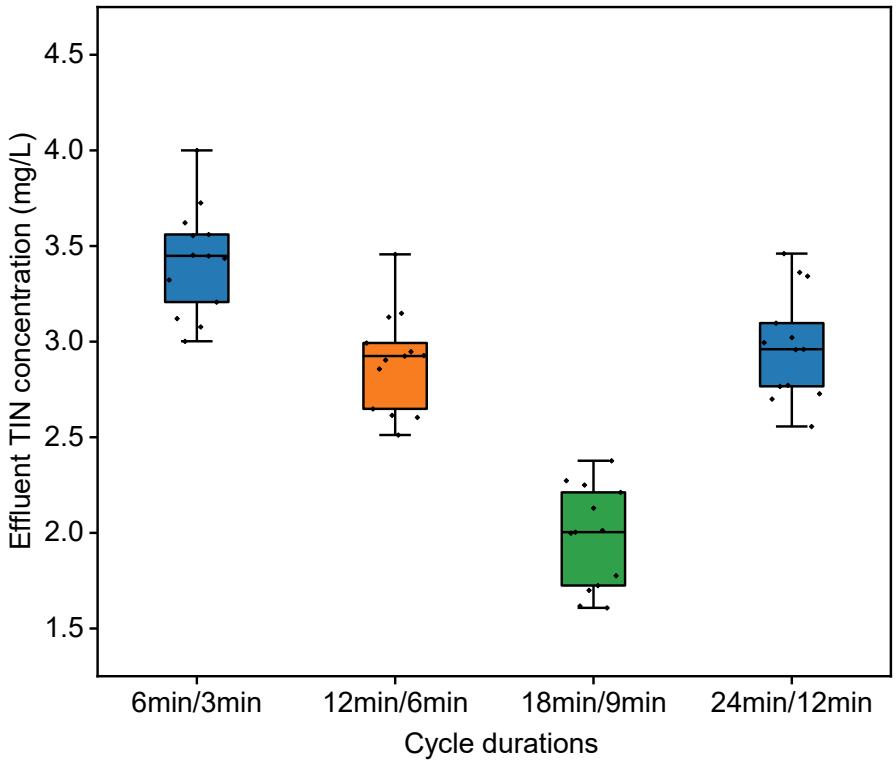


Fig. S1 Effluent TIN concentrations under different cycle durations.

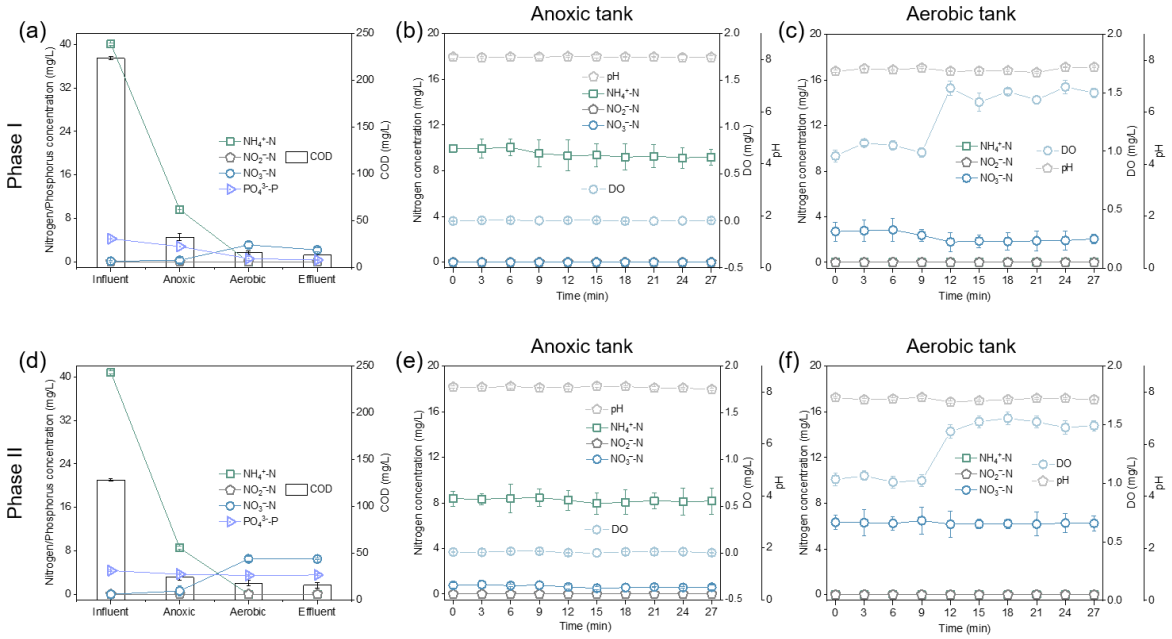


Fig. S2 The nitrogen, phosphorus and COD profiles in the anoxic and oxic tanks of the novel continuous A/O process over a typical cycle in Phase I and Phase II.

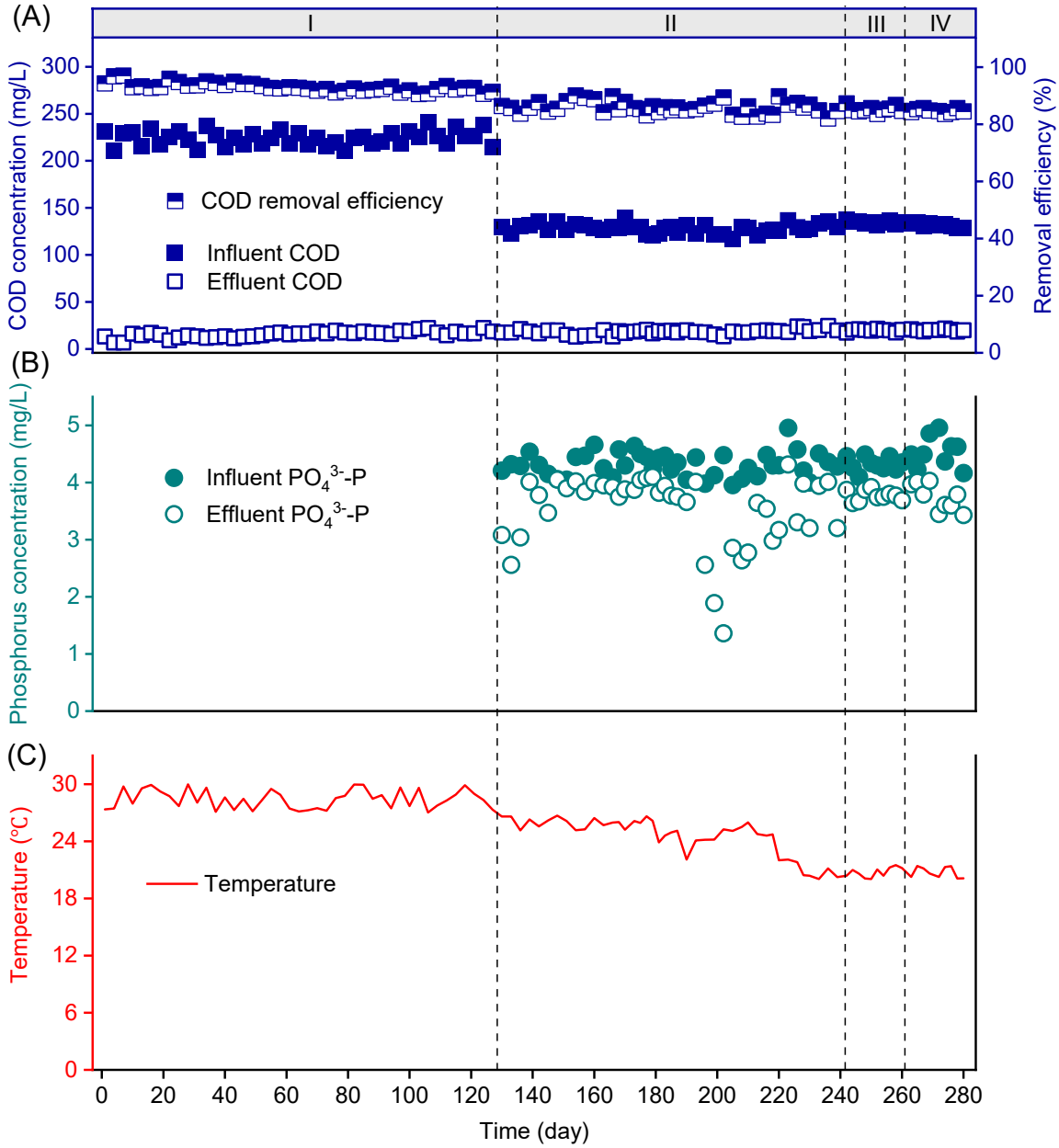


Fig. S3 Reactor performance during the operation of 280 days. (a) The influent, effluent, and removal efficiency of COD; **(b)** The influent and effluent PO_4^{3-}-P; **(c)** The operating temperatures.

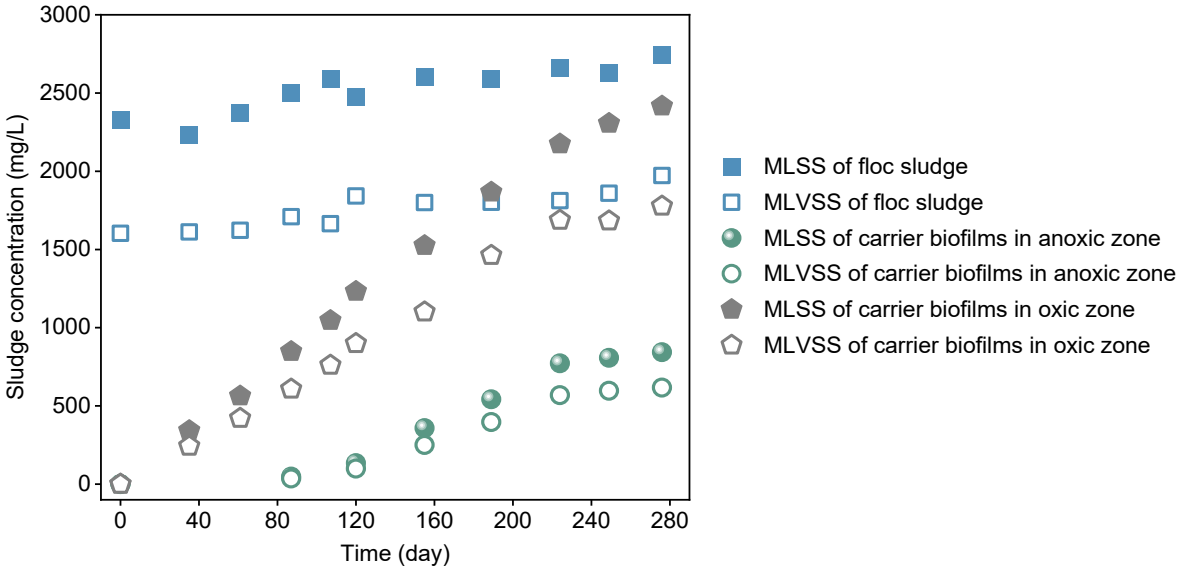


Fig. S4 The sludge concentrations of suspended sludge and carrier biofilms

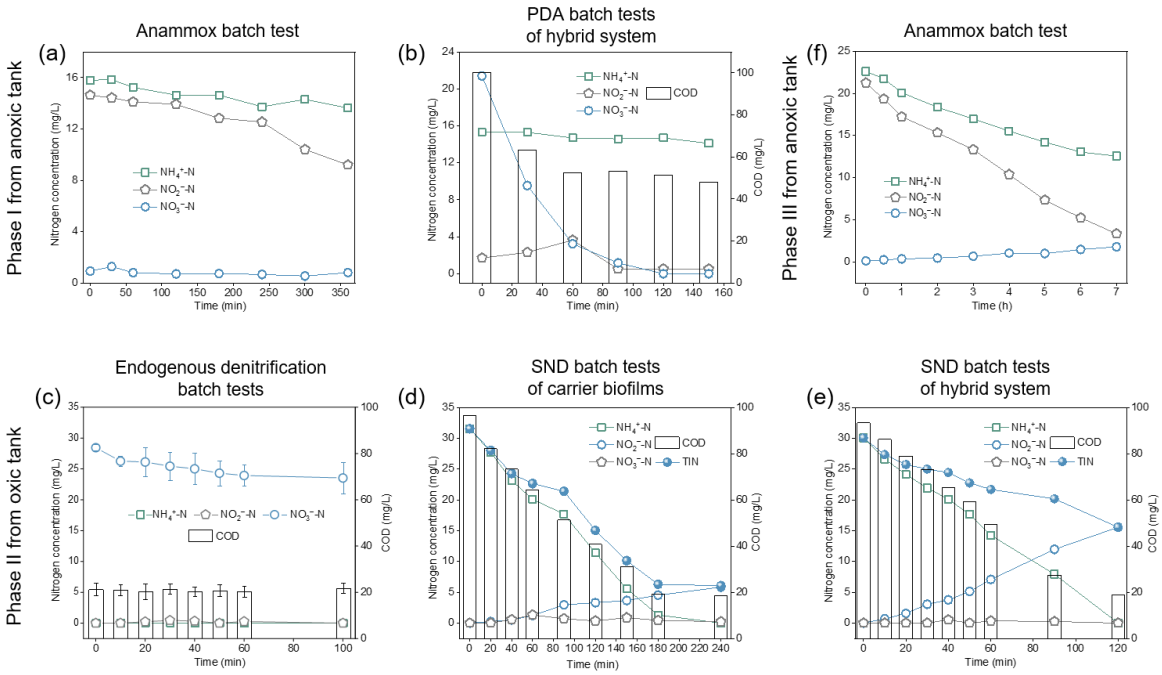


Fig. S5 Specific variations of nitrogen and COD in batch tests. (a) The anammox batch tests of anoxic biofilms in Phase I; **(b)** The PDA batch tests of hybrid system from anoxic zone in Phase I; **(c)** The endogenous denitrification batch tests of suspended sludge in Phase II; **(d)** The SND batch tests of carrier biofilms from oxic zone in Phase II; **(e)** The SND batch tests of hybrid system from oxic zone in Phase II; **(f)** The anammox batch tests of anoxic biofilms in Phase III. (Note: Hybrid systems comprised both carrier biofilms and suspended sludge. Samples used for batch tests were collected on day 105 for Phase I, day 220 for Phase II, and day 250 for Phase III.)

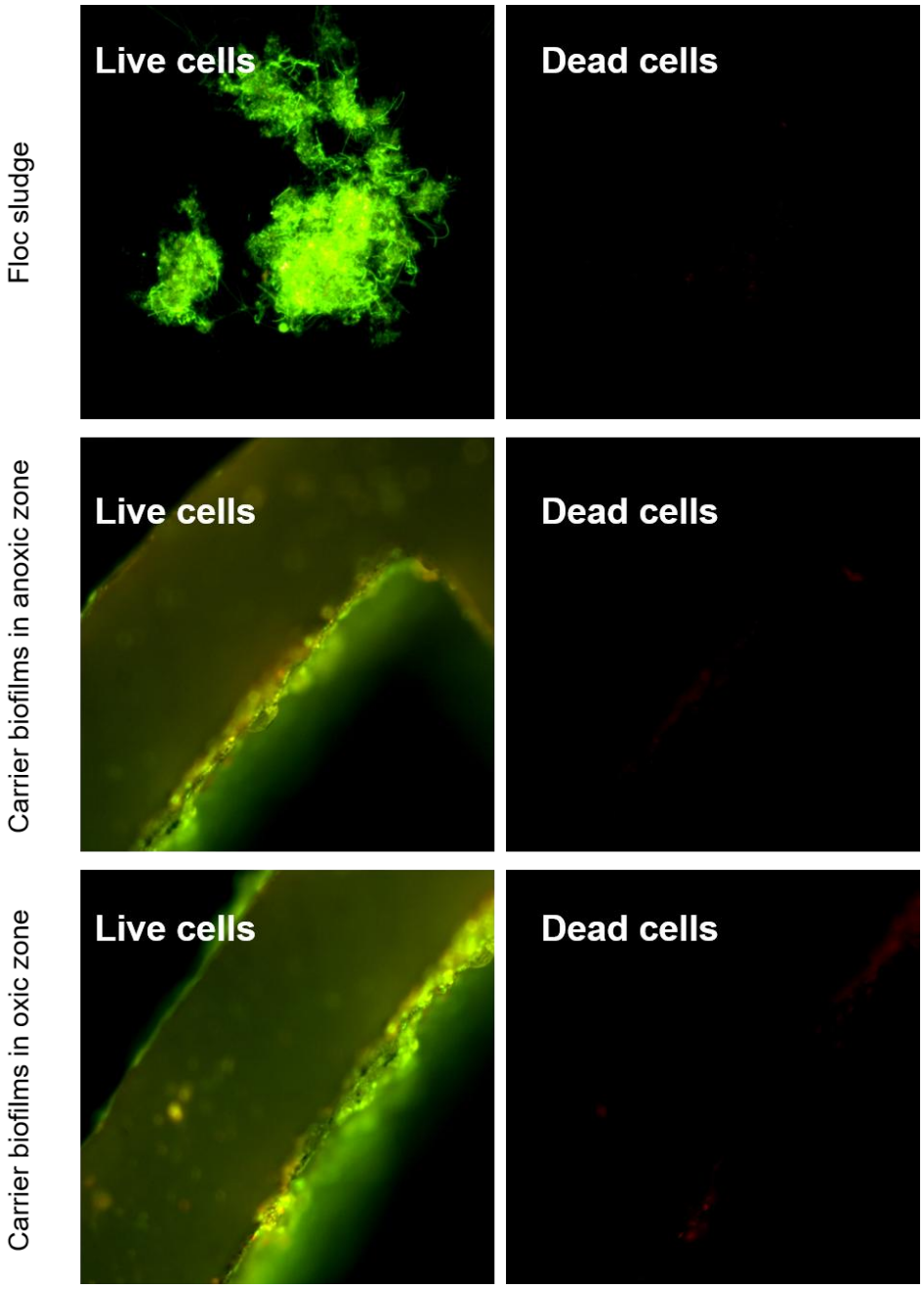


Fig. S6 Microscopic visualization of suspended sludge and carrier biofilms based on the fluorescence images of live (green) and dead (red) cells.

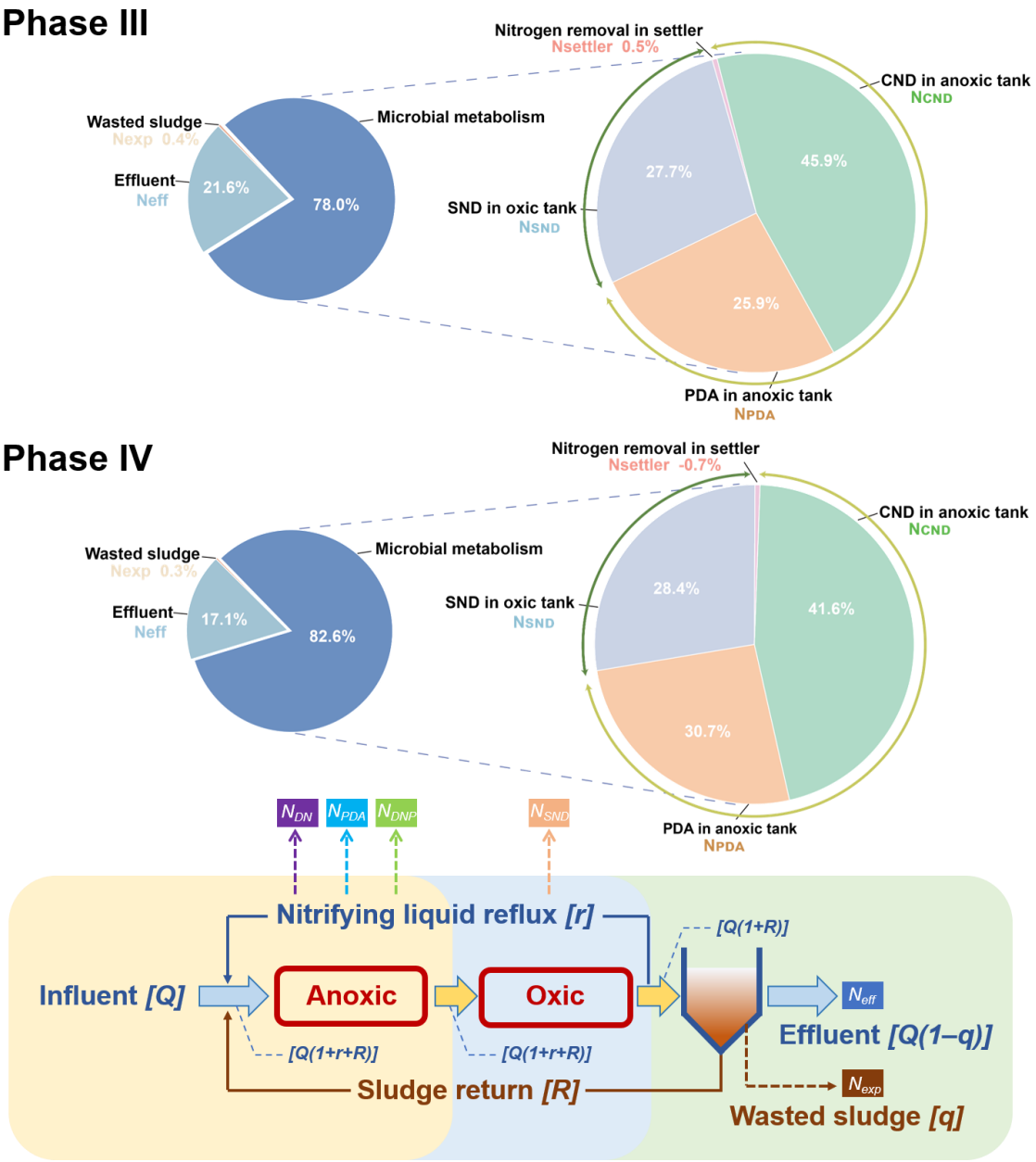


Fig. S7 Mass balance calculations for nitrogen in Phase III and Phase IV of the novel modified continuous A/O process. *r*: nitrifying liquid reflux ratio [%]; *R*: sludge return ratio [%]; *q*: wasted sludge ratio [%]; *Q*: average influent flowrate [L/d]; N_{exp}: TIN in the wasted sludge; N_{eff}: TIN in the effluent; N_{PDA}: nitrogen loss by PDA; N_{SND}: nitrogen loss by SND; N_{CND}: nitrogen loss by CND in anoxic tank; $N_{settler}$: nitrogen in settler.

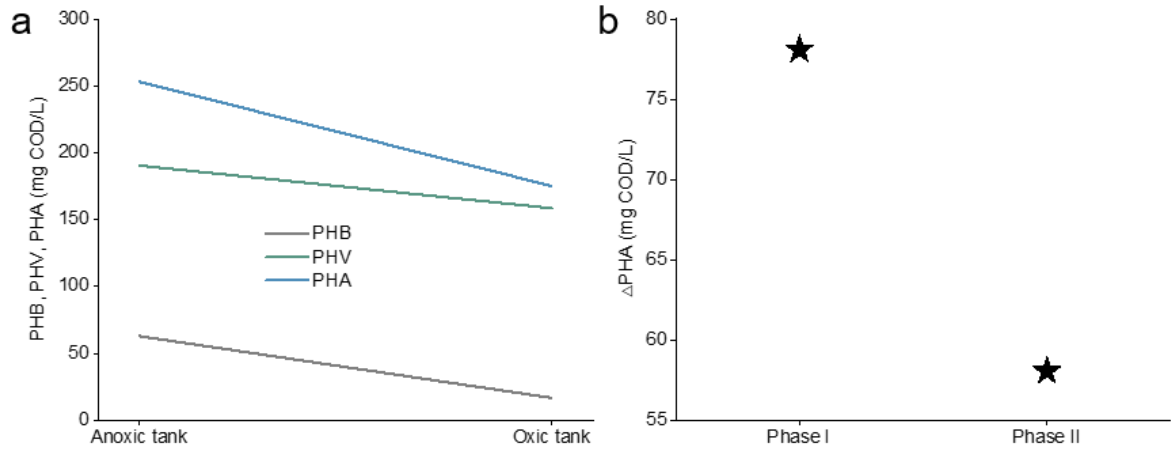


Fig. S8 Evolution of intracellular carbon sources. (a) The conversion of endogenous carbon sources (PHA, PHB, PHV) from anoxic tank to oxic tank; **(b)** Variations in the amount of PHA in phase I and phase II.

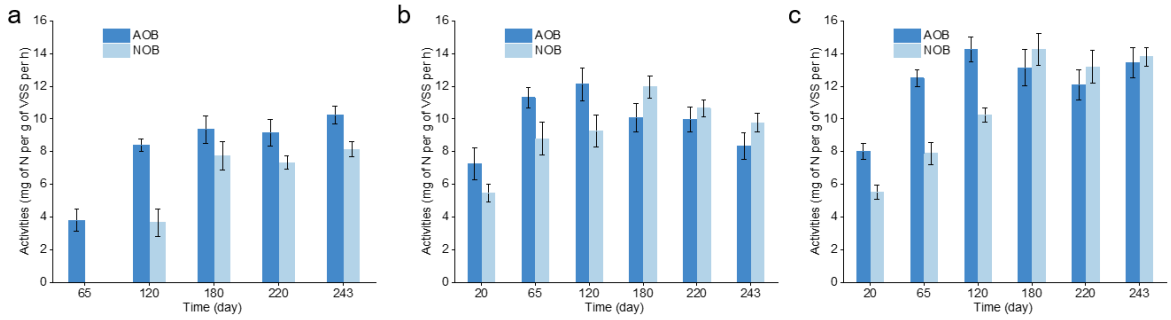


Fig. S9 Variation in the nitrification activity in the reactor. (a) Nitrification activity of aerobic carrier biofilms; **(b)** Nitrification activity of suspended sludge; **(c)** Nitrification activity of the hybrid system. (Note: the hybrid system contained aerobic carrier biofilms and suspended sludge.)

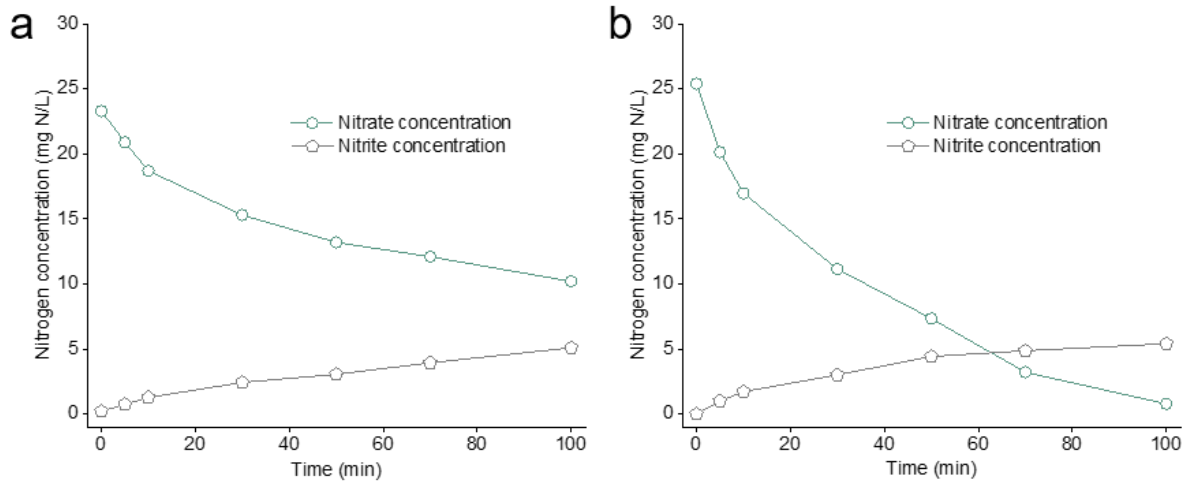


Fig. S10 Denitrification batch tests of the carrier biofilms (a) and the hybrid system (b) from anoxic tank. (Note: the hybrid system contained anoxic carrier biofilms and suspended sludge. Samples used for batch tests were collected on day 220.)

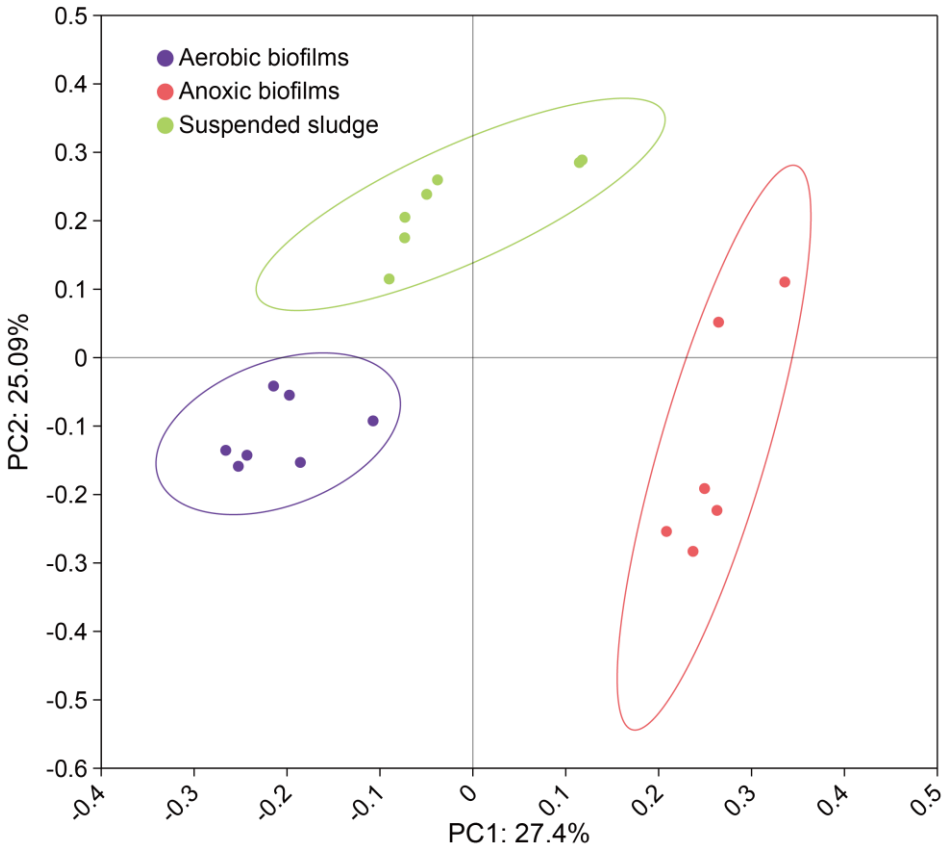


Fig. S11 Results of the principal coordinates analysis (PCoA) at the ASV level.

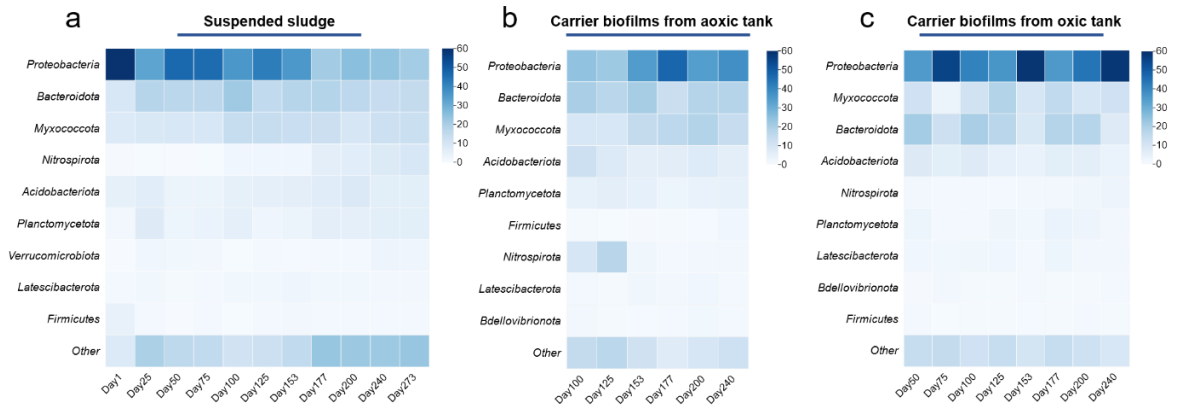


Fig. S12 Microbial community structure at the phylum level from suspended sludge (a), carrier biofilms from anoxic tank (b) and oxic tank (c).

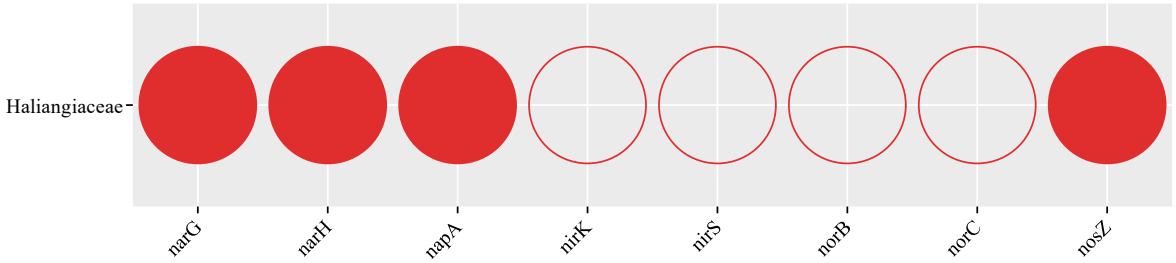


Fig. S13 Profile of the nitrogen-cycle genes in *Haliangiaceae* genome.

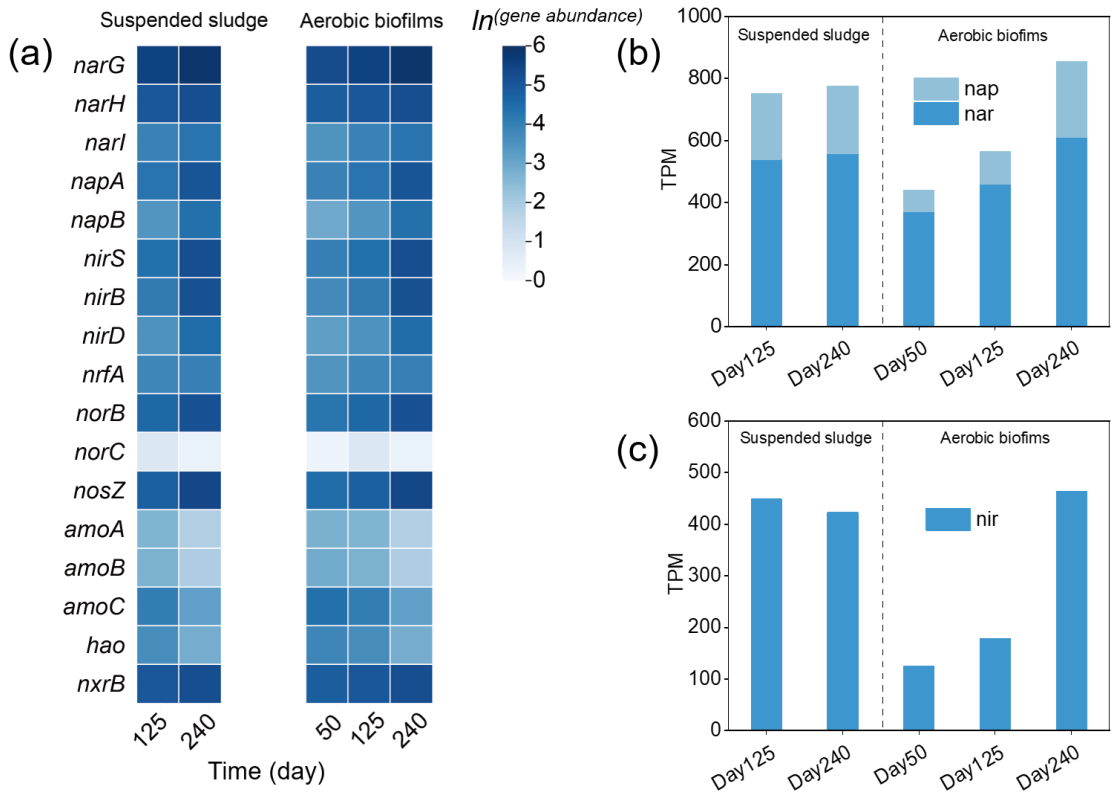


Fig. S14 The key genes involved in denitrification and nitrification processes in suspended sludge and aerobic biofilms. (a) Variations in the relative abundance of functional genes. **(b)** Variations in the relative abundance of *nar* and *nap* genes in suspended sludge and aerobic biofilms. **(c)** Variations in the relative abundance of *nir* genes in suspended sludge and aerobic biofilms.

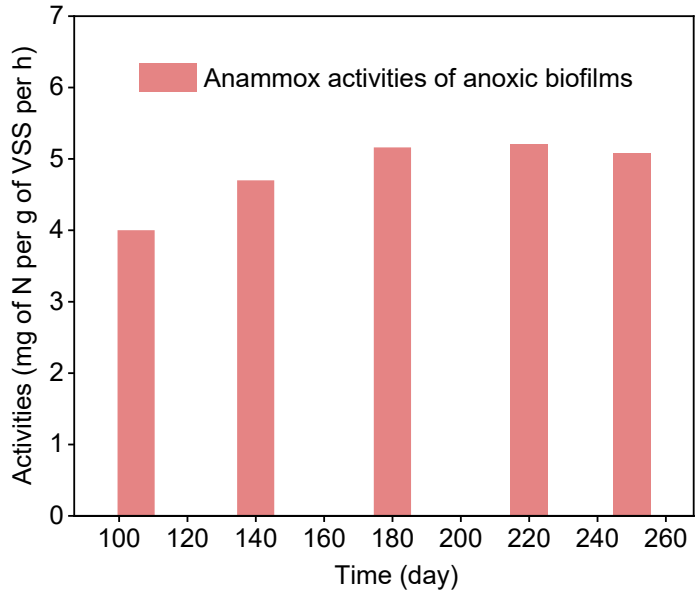


Fig. S15 Long-term dynamics of anammox activity in anoxic biofilms.

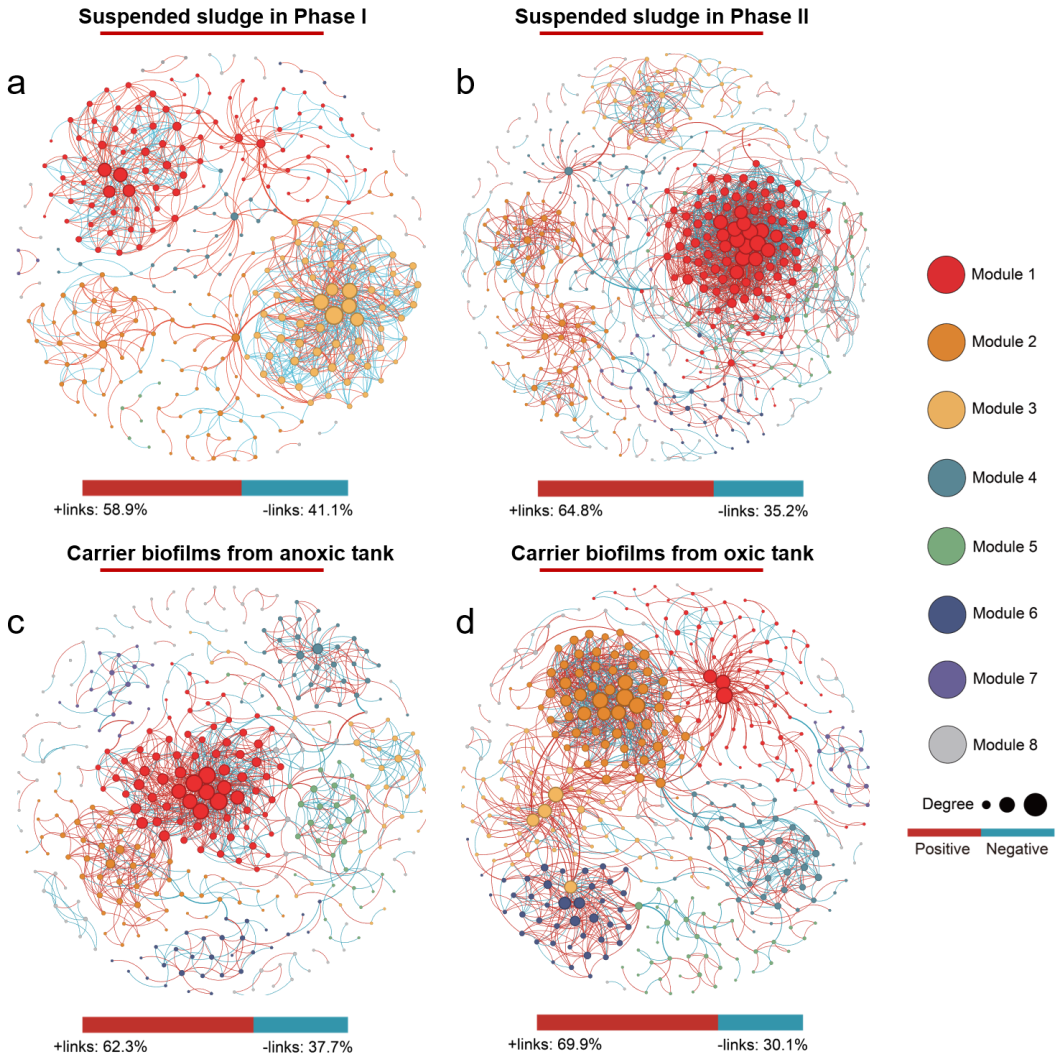


Fig. S16 Bacterial co-occurrence networks constructed from ASV-level Spearman correlations. Networks were generated based on pairwise Spearman correlation coefficients ($|r| > 0.7$, $P < 0.01$) among ASVs. Node size reflects the degree of connectivity (i.e., the number of significant associations). The top panels depict microbial interaction networks from suspended sludge in Phase I **(a)** and Phase II **(b)**, while the bottom panels illustrate those from anoxic **(c)** and oxic **(d)** biofilms.

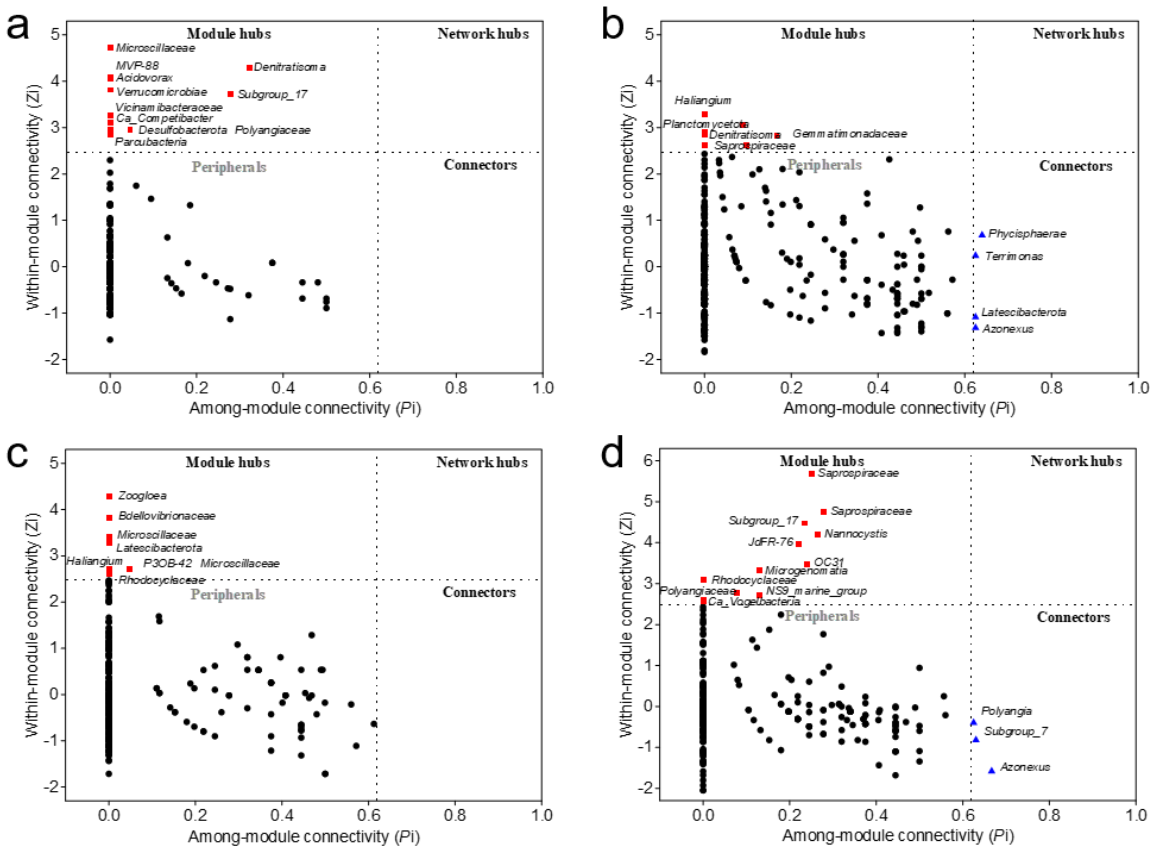


Fig. S17 Z−P plot of ASVs in microbiomes based on their topological roles. (a) Z−P plot of ASVs in suspended sludge from phase I. **(b)** Z−P plot of ASVs in suspended sludge from phase II. **(c)** Z−P plot of ASVs in anaerobic carrier biofilms. **(d)** Z−P plot of ASVs in aerobic carrier biofilms. The topological feature of each node was determined based on the scatter patterns of Zi and Pi.

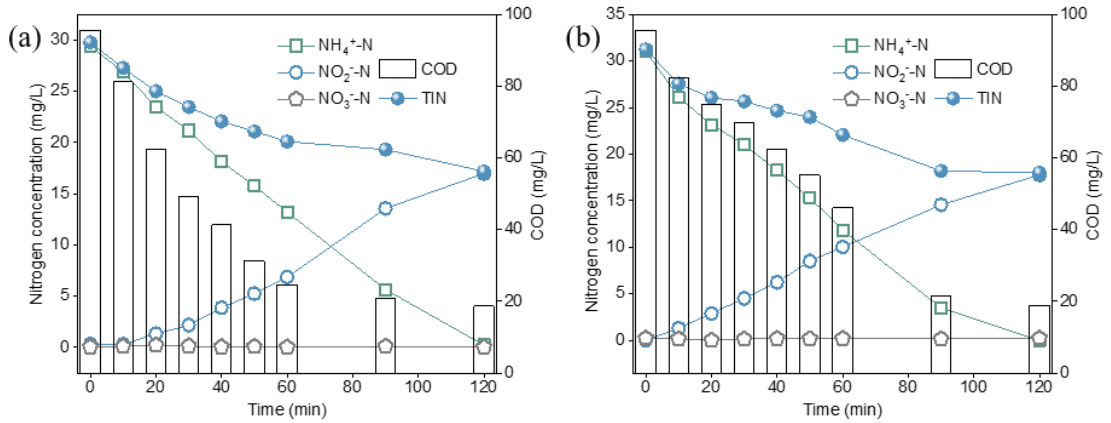


Fig. S18 SND batch tests conducted at a dissolved oxygen concentration of 1.4-1.5 mg O_2/L. (a) SND activity of hybrid system from oxic tank in Phase I; **(b)** SND activity of hybrid system from oxic tank in Phase II. (Note: Hybrid systems comprised both carrier biofilms and suspended sludge. Samples used for batch tests were collected on day 105 for Phase I and on day 220 for Phase II.)

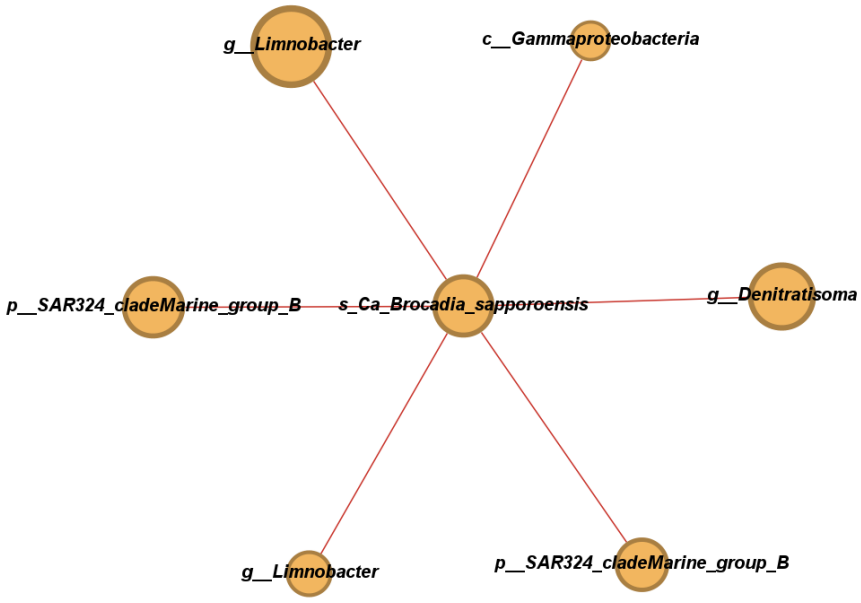


Fig. S19 Microbial co-occurrence networks of specie *Ca. Brocadia sapporoensis* based on pairwise Spearman's correlations among ASVs. With only significant associations ($P < 0.01$ and correlation coefficient >|0.7|) included. Nodes size is scaled according to the number of connections (degree).

References:

Alneberg J, Bjarnason B S, De Bruijn I, Schirmer M, Quick J, Ijaz U Z, Lahti L, Loman N J, Andersson A F, Quince C (2014). Binning metagenomic contigs by coverage and composition. Nat Methods, 11(11): 1144-1146

Bolger A M, Lohse M, Usadel B (2014). Trimmomatic: a flexible trimmer for Illumina sequence data. Bioinformatics, 30(15): 2114-2120

Chaumeil P-A, Mussig A J, Hugenholtz P, Parks D H, Hancock J (2020). GTDB-Tk: a toolkit to classify genomes with the Genome Taxonomy Database. Bioinformatics, 36(6): 1925-1927

Hyatt D, Chen G L, Locascio P F, Land M L, Larimer F W, Hauser L J (2010). Prodigal: prokaryotic gene recognition and translation initiation site identification. BMC Bioinformatics, 11: 119

Meng Q, Zeng W, Wang B, Fan Z, Peng Y (2020). New insights in the competition of polyphosphate-accumulating organisms and glycogen-accumulating organisms under glycogen accumulating metabolism with trace Poly-P using flow cytometry. Chemical Engineering Journal, 385

Olm M R, Brown C T, Brooks B, Banfield J F (2017). dRep: a tool for fast and accurate genomic comparisons that enables improved genome recovery from metagenomes through de-replication. ISME J, 11(12): 2864-2868

Parks D H, Chuvochina M, Rinke C, Mussig A J, Chaumeil P A, Hugenholtz P (2022). GTDB: an ongoing census of bacterial and archaeal diversity through a phylogenetically consistent, rank normalized and complete genome-based taxonomy. Nucleic Acids Res, 50(D1): D785-D794

Tu Q, Lin L, Cheng L, Deng Y, He Z, Wren J (2019). NCycDB: a curated integrative database for fast and accurate metagenomic profiling of nitrogen cycling genes. Bioinformatics, 35(6): 1040-1048

Wu Y-W, Simmons B A, Singer S W (2016). MaxBin 2.0: an automated binning algorithm to recover genomes from multiple metagenomic datasets. Bioinformatics, 32(4): 605-607

Yuan S, Guo S, Huang X, Meng F (2022). Time-lagged interspecies interactions prevail during biofilm development in moving bed biofilm reactor. Biotechnol Bioeng, 119(10): 2770-2783